DROP IMPACTS IN POOLS: A COMPARISION BETWEEN HIGH SPEED IMAGING AND NUMERICAL SIMULATIONS

S. Fest-Santini*, M. Guilizzoni°, M. Santini*, G.E. Cossali*

* Department of Industrial Engineering, University of Bergamo, viale Marconi 5, 24044 Dalmine (BG), Italy
° Department of Energy, Politecnico di Milano, via Lambruschini 4, 20156 Milan, Italy

ABSTRACT
A feasibility study is done aimed at verifying the capabilities of the open source CFD package OpenFOAM® to predict the dynamic crater evolution and accompanying phenomena during drop impact into deep pools in the cratering regime. Two experimental test cases are chosen, whose crater evolutions are in one case influenced and in the other not influenced by wall effects, so that 2D and 3D domain geometries are respectively required. OpenFOAM® seems to be a promising tool to predict drop impacts already with standard solver settings, even if the finest and most dynamic accompanying phenomena, which also can affect the crater shape, could not be correctly predicted. This may be due to limits in the implemented models and to memory and, thereby, mesh limitations with the present numerical set-up.

INTRODUCTION

The cratering regime with his manifold characteristics like micro-entrapments [1], primary entrapment which could lead to the trampoline phenomena [2], vortex rings [3], micro-jetting [4] and thick jets [5] is chosen as a study case for a comparison between high speed imaging and numerical simulations. This study is aimed at verifying the capabilities of CFD software packages as they are, with simple settings and performing simulations on a common personal computer without the need for a cluster. The OpenFOAM® open source CFD package was selected because of its large community of users and successful examples of use of its two-phase *interFoam* solver in the fields of drop splashing and impact as reported in literature [6-9].

Two characteristic drop impacts which feature micro-entrapments, primary entrapment and trampoline phenomena are selected as test cases. Hereby, the impact points are varied. One impact point is fixed far enough from the pool walls that the latter have no influence on the crater evolution. On the contrary in the second test case, the distance between the impact point and the camera-facing pool wall is reduced, so that wall effects on the crater evolution can only be neglected for the initial stage of drop impact. The benefit of the reduced distance between impact point and wall is that it allows a much more detailed observation of the phenomena happening within the droplet, as shown in fig. 1.

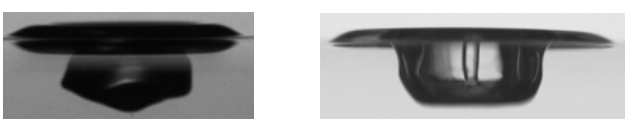

Figure 1: Differences in the experimentally obtained level of detail for the two test cases: crater evolution without (left) and with (right) wall effect for later stage of drop impact.

MATERIAL AND METHODS

Experimental procedure

Drop impact experiments are carried out at the Department of Industrial Engineering, University of Bergamo, whereby the high-speed visualisation techniques with continuous back-light illumination is used to observe droplet impacts into a pool of the same liquid. Water droplets of millimetric size are produced with an on-demand droplet generator. Droplets exiting the generator are accelerated by gravity and impact in the pool, whose horizontal alignment is achieved by a 6-jack platform with precision of ±10 μrad.

Special accuracy is required in the alignment of pool's water level and camera position in relation to the water level. Otherwise, refractive and alignment distortions or black stripes within the images due to liquid interfacial phenomena with the pool walls (meniscus) appear. It is worth noting that the dimension of black stripes depends also from the thickness of the pool walls and can only be avoided by a correct and constant water level in the pool. Thereby, the pool is connected to a level water container mounted on a micrometric stage. The micrometric stage allows a precise regulation of the water level, whereby the large surface area of the level pool guaranties its constancy during experiments. Additionally, the camera is mounted on a tilting, rotating and movable platform, so that its lens axis can be independently adjusted.

The recorded images are post-processed to obtain the crater interface as function of time. Hereby, the algorithm comprises background subtraction, contrast enhancement, image cleaning and edge detection using the Laplacian of Gaussian (LoG) method and feature detection. The contrast enhancement including lower and high upper limits of the

intensities setting and the intensification factor are adapted to the detected information. Each experimental investigation is analysed by extracting the following information: (a) impact velocity and diameter using the frames before drop impact, (b) crater interface contour as function of time and (c) the contour of entrapped air bubbles as a function of time. The extracted crater interfaces are used to calculate crater depths and widths for each recorded time step after impact. Velocity trajectories of the micro-entrapments, which are detected during the early stage of drop impact, are calculated from their extracted contours.

Numerical simulations

Numerical simulations are performed at the Department of Energy, Politecnico di Milano, using the finite volume two-phase solver *interFoam* of the OpenFOAM® 1.7.1 open source CFD toolbox distributed by OpenCFD® Ltd. The solver implements an improved Volume of Fluid (VOF) model based on a two-fluid approach, with the continuum surface force (CSF) model to include surface tension at the interface. Interface compression is performed to get a sharper contour between the phases. Coherently with the scope of this work, standard solver setting and no adaptive grid refinement are used. The surrounding air, the drop and pool water are assumed Newtonian and incompressible and the flow laminar. For each phase the values of all relevant thermophysical properties are taken at the respective temperature measured during the experiments. Initial positions and conditions of the two phases are fixed using the *setFields* and *funkySetFields* OpenFOAM® utilities.

2D axisymmetric simulations are performed in the study of the case without wall effects and 3D domains are considered - exploiting symmetry planes where possible - for the second study case, where wall effects need to be taken into account during the later stage of drop impact. For axisymmetric simulations, the drop is let fall from a height corresponding to the experimental one. To reduce the domain dimensions, in 3D simulations the drop is on the contrary directly placed near the free surface of the pool with an initial velocity equal to the one it would reach falling from the corresponding experimental height (neglecting air drag).

In both cases the mesh is structured, made by rectangular hexahedra in the 3D case, by wedges in the axisymmetric case. The number of cells and the average cell volume (cell area in the axisymmetric case) are reported in tab. 1.

In general, the mesh is graded at least in one direction, so that the cell volume is not uniform. Different meshes are tested to analyse the sensitivity of the solution to the mesh size and their details are summarised in tab. 1.

Table 1: Mesh details for the 2D axisymmetric and 3D domains. The colours correspond to the ones used to trace the boundary between the phases in figs. 3 and 5.

Case code	Cell. Number ($\cdot 10^{-6}$)	Domain extension [m] (D x W x H)	Domain volume [m^3]	Avg.cell. volume [m^3]
3D-C	4.200	0.040 x 0.030 x 0.014	1.68e-05	4.00e-12
3D-I	4.608	0.018 x 0.012 x 0.012	2.59e-06	5.62e-13
3D-I				
3D-F	5.400	0.015 x 0.009 x 0.009	1.22e-06	2.25e-13
2D	1.000	0.020 x 0.025	5.00e-04	5.00e-10

The boundary conditions are defined as follows:

- wall boundary for the front, back, bottom and external sides of the pool;
- open boundary for the top of the domain ("atmosphere");
- axial symmetry for the axis in the axisymmetric case and
- symmetry plane for the internal "side" of the mid-pool in the 3D case.

The time step is adapted by the solver to keep the Courant number under 0.5 and to output the solution at the desired time intervals matched to the experimental time steps.

Figure 2 shows the two domains with the corresponding initial configuration of the phases.

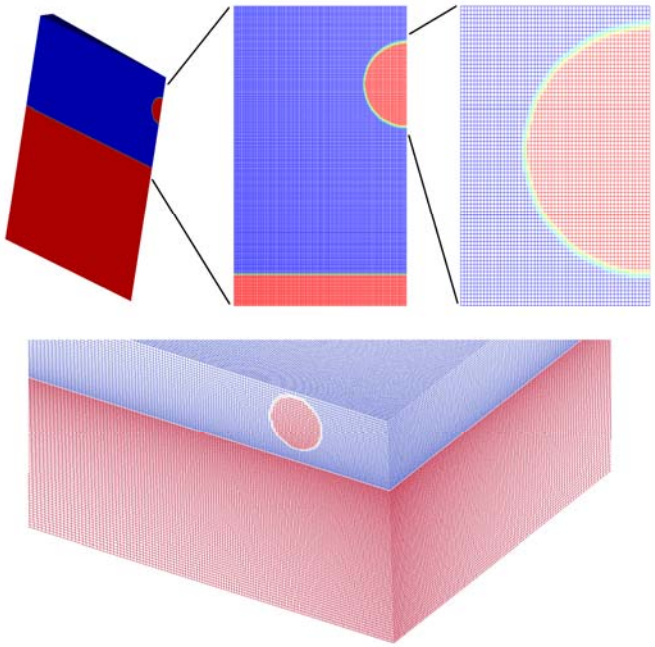

Figure 2: Mesh and initial configuration of the phases for the two investigated test cases

RESULTS

Crater evolution without wall effect

In fig. 3, the phase contours of the numerically simulated axisymmetric drop impact are superposed to the experimentally obtained images, showing a quite good qualitative agreement. While the crater is formed in the target liquid, a swell rises up on its base and propagates on the liquid surface. This quite thick rim is slightly overestimated in terms of initial height and elongation. The elongation overestimation becomes more pronounced with increasing time after impact. On the contrary, the crater contour is well described at the initial and final stage of drop impact, whereas the intermediate stage of the crater evolution dynamic is affected by the trampoline phenomena. A series of capillary waves propagates up the impacting drop and converges at its top, pinching off a smaller secondary drop. As shown in more detail in fig. 5, the secondary drop falls onto the bottom of the crater and is then ejected by the receding crater. This phenomenon could not be captured by the simulations and consequently the simulated crater contour does not reflect the characteristic crater shape. In preliminary simulations of other cases, secondary drop ejection was obtained. Therefore the failure in the present case may be due to the rough capture of the crater shape at the end of its deepening, which influences its retraction and trampoline behaviour.

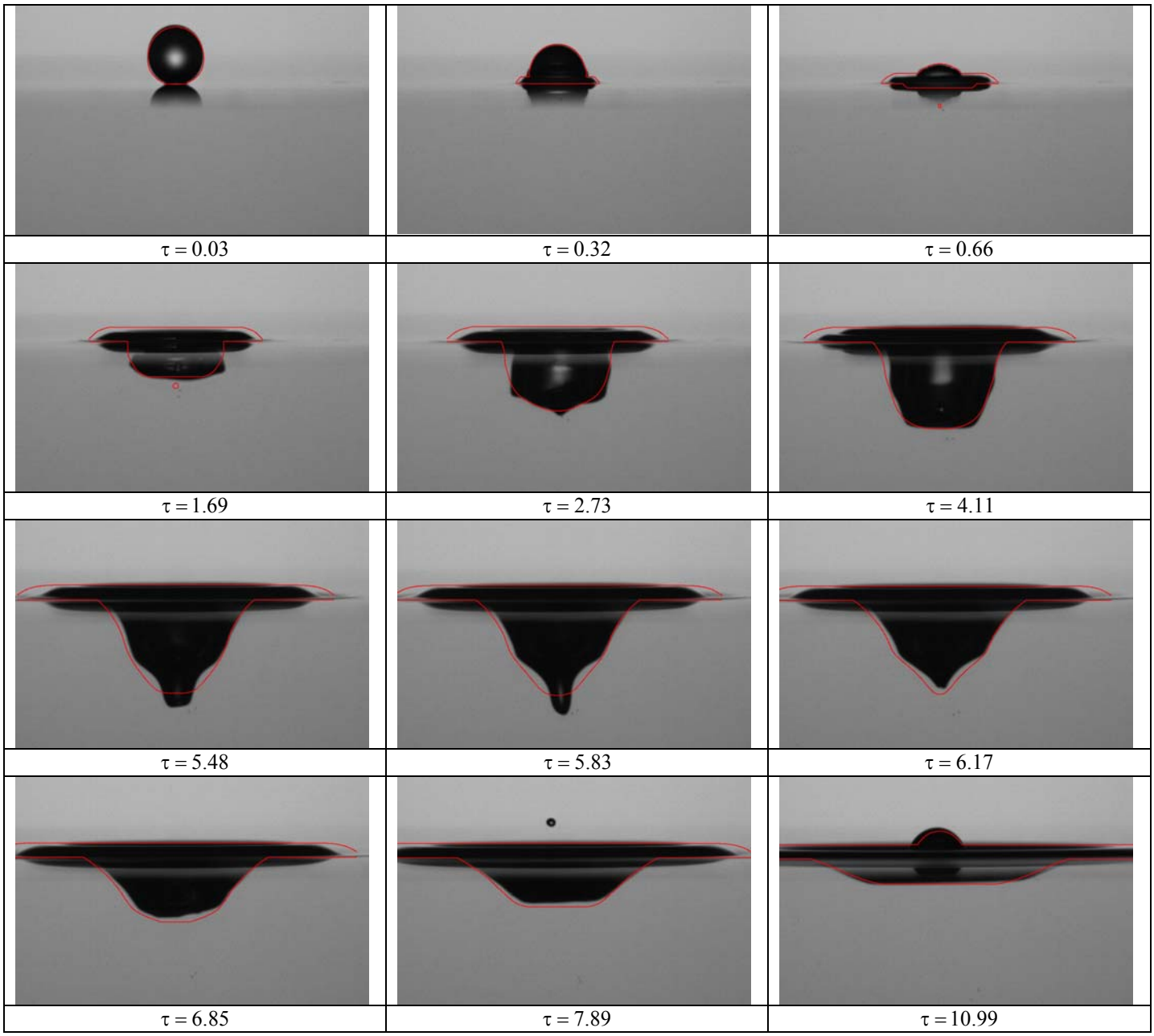

Figure 3: Superposition of experimentally [2] and numerically obtained dynamic crater evolution in the cratering regime (d = 2.8 mm, v = 1.24 m/s, We = 54, Fr = 52).

The final stage of drop impact, which is characterised by the formation of a dome, is described in well agreement with the experimental data.

Crater evolution with wall effects

The distance between the wall and the drop impact point is reduced to be able to capture in the experimental images more details about the phenomena within the drop. As already mentioned, the crater evolution is influenced by the presence of the camera-facing pool wall, as it is shown for example in fig. 4. A 3D-simulation approach is required and consequently, more computer resources are needed. Thereby, different domain sizes, cell sizes and cell numbers are analysed as reported in tab. 1. With decreasing cell size, the required time step becomes smaller to respect the limit on the Courant number, so that the simulation time suffers from a significant increase. Simulations with finer mesh are therefore performed only for initial stage of drop impact, whose solution depends significantly from the mesh. For example, the coarser mesh - indicated in blue in fig. 5 - does not capture the entrapped micro-bubbles.

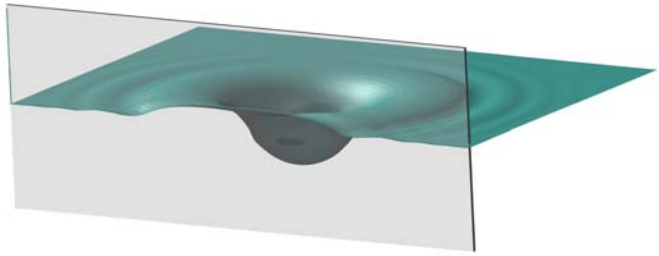

Figure 4: A simulated frame (rendered using POV-Ray®) showing the influence of the camera-facing pool wall on the crater evolution.

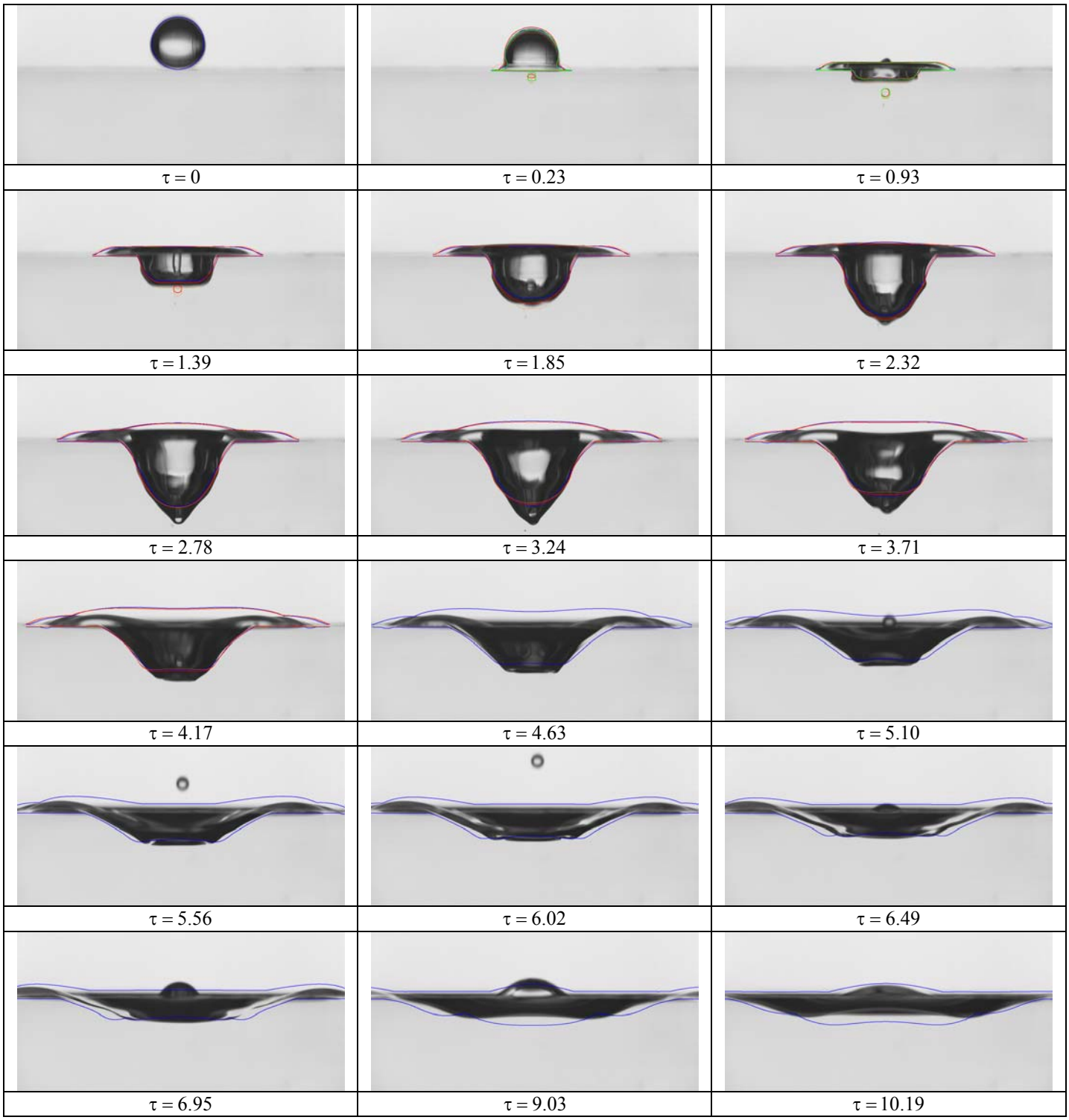

Figure 5: Superposition of experimentally and numerically obtained dynamic crater evolution influenced by camera-facing pool wall in the cratering regime (d = 3.35 mm, v = 0.81 m/s, We = 31, Fr = 20). Different mesh sizes are used as summarised in Tab. 1.

As already reported for the 2D simulation, the trampoline phenomena could not be predicted. Thereby, the numerically obtained crater shape differs in terms of depth as well as rim height with respect to the pool surface. In summary, all the different meshing strategies lead to an underestimation of the maximum crater depth and an overestimation of the maximum crater width. For a correct evaluation of the simulation performances, it must be also underlined that a significant problem is the correct superposition of the numerical results on the experimental frames. Difficulties arise from different refraction indexes between air and water and results in different scales of the droplet in air and water. Moreover, a major issue is that synchronization is done manually by measuring the distance of the drop from the pool free surface in a suitable picture and converting it into a distance which is used for initialization of the drop position in the simulations. The same principle holds for the determination of the drop diameter and shape. Unfortunately, a small error in these parameters has a significant influence on the results: as an example, for case H40I the red and the orange contours represent results from the same simulation but the latter shows the contours half an experimental time step after the red ones.

Figure 6 shows the comparison between the experimentally detected and numerically predicted crater width and depth. It

can be noticed how the agreement reflects the above mentioned considerations and is fairly good in the case of the axisymmetric simulation, while for the 3D larger deviations are observed.

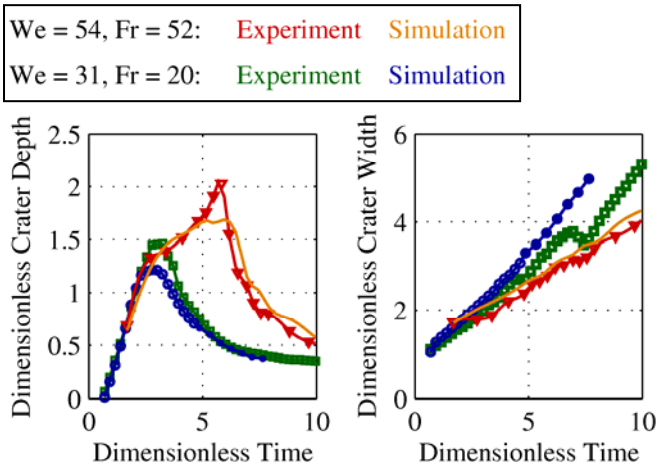

Figure 6: Comparison between the experimentally detected and numerically predicted crater width and depth.

Micro-entrapment

At the initial stage of drop impacts, micro air bubbles can be formed, when a thin air sheet remains entrapped between the two contacting liquid surfaces. For the dimensionless time step $\tau = 0.23$ of fig. 5, the two observed micro-bubbles are highlighted in fig. 7. They feature an average size of 0.03 mm². In fig. 7, their droplet contours and the corresponding velocity vectors are plotted with respect to their impact point . The upper micro-entrapment, pointed out in blue, seems to be influenced by the crater evolution; the lower bubble, marked in green, may be decelerated by the bulk liquid. The propagation direction of both is properly affected by a vortex ring visible dying the impacting drop [2].

The phenomena of entrapment and rupture of a thin air sheet is also captured in the 2D and 3D simulations, even if the agreement with the experimental observations is only qualitative. Figures 8 and 9 show how air is trapped under the drop and the dynamics of the resulting bubble, “chased” by the crater which in the end reaches and captures it. The simulation may offer an insight of what happens (fig. 9): the thin film of trapped air, stretched during the impact, retracts due to surface tension thus creating an initially "eight-shaped" bubble. If the bubble neck becomes too thin, fragmentation in two bubbles occurs. Otherwise the bubble evolves towards more spherical shapes.

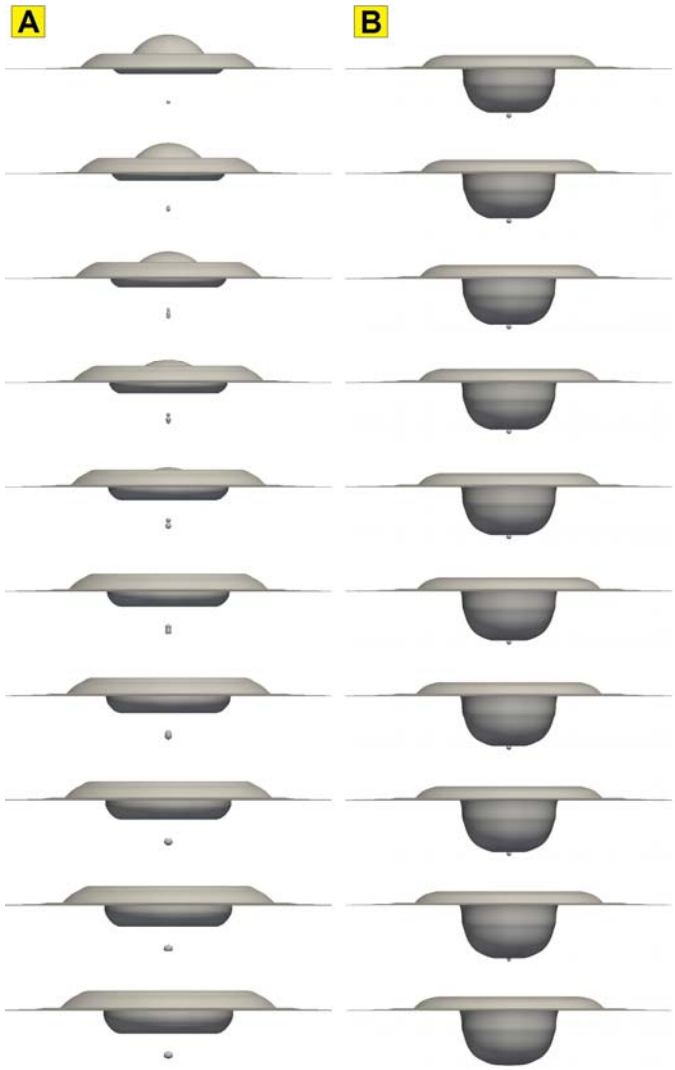

Figure 8: Dynamics of the air trapped under the crater, which at the end is reached and captured by it. The time step between the frames in each sequence is $1e^{-4}$ s.

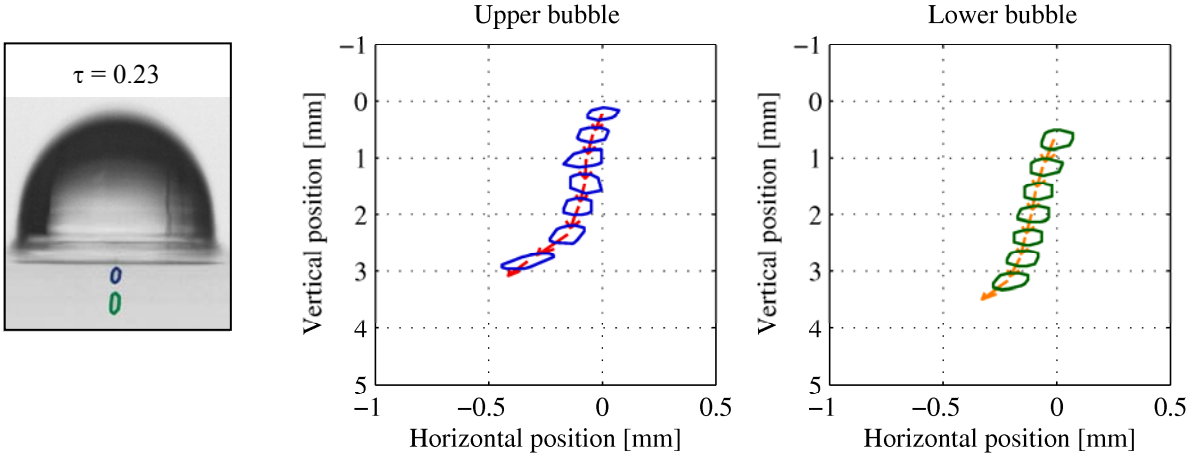

Figure 7: Contour and velocity vector of micro-entrapments at the initial stage of drop impact

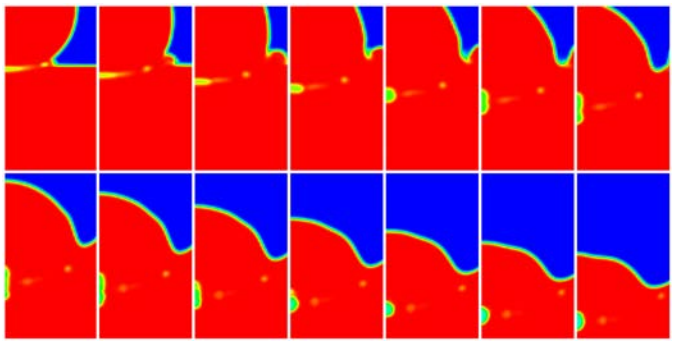

Figure 9: Details of the air dynamics (green region) in the first instants after the drop impact. The time step between the frames is $2e^{-4}$ s.

CONCLUSIONS

A comparative study of experimentally and numerically obtained drop impacts into deep pools in the cratering regime was performed. The feasibility of the use of the *interFoam* solver of the OpenFOAM® CFD toolbox was tested using "default" solver settings, basic meshing of the domain and a standard personal computer. The *interFoam* solver seems to be a very promising tool for the simulation of drop impacts into pools, although the highly dynamic processes like the trampoline phenomena could not be numerically predicted. Probably, the description of these phenomena requires a finer mesh, whose size was actually limited by the available memory. Thereby, it is planned to refine statically or adaptively the mesh geometry and to use a cluster. Furthermore, the analysis will be extended to the influence of the impacting drop shape.

NOMENCLATURE

Symbol	Quantity	SI Unit
d	diameter	m
Fr	Froude numer	-
v	velocity	m/s
We	Weber number	-
τ	dimensionless time	.

REFERENCES

[1] S.T. Thoroddsen, T.G. Etoh, K. Takehara, Air entrapment under an impacting drop, *J. Fluid Mech.*, vol. 478, pp. 125–134, 2003

[2] A. Bisighini, Single and double drop impact onto a deep and thick liquid layer, Ph.D. Thesis, University of Bergamo, 2009

[3] F. Rodriguez, R. Mesler, The penetration of drop-formed vortex rings into pools of liquid, *J. Coll. Int. Sci.*, vol. 121 (1), pp. 121-129, 1988

[4] M. Rein. The transitional regime between coalescing and splashing drops. *J. Fluid Mech.*, vol. 306, pp. 145–165, 1996.

[5] J.L. Liow, Splash formation by spherical drops, *J. Fluid Mech.*, vol. 427, pp. 73–105, 2001

[6]. Berberović, N.P. van Hinsberg, S. Jakirlić, I.V. Roisman, C. Tropea, Drop impact onto a liquid layer of finite thickness: Dynamics of the cavity evolution, *Phys. Rev. E 79*, 036306, 2009

[7] A.B. Costa, R. Graham Cooks, Simulated splashes: Elucidating the mechanism of desorption electrospray ionization mass spectrometry, *Chemical Physics Letters*, vol. 464, pp. 1-8, 2008

[8] I.V. Roisman, C.M. Weickgenannt, A.N. Lembach, and C. Tropea, Drop impact close to a pore: experimental and numerical investigations, *23rd Annual Conference on Liquid Atomization and Spray Systems*, Brno, Czech Republic, September 2010

[9] E. Berberović, Investigation of Free-surface Flow Associated with Drop Impact: Numerical Simulations and Theoretical Modeling, Ph.D. Thesis, TU Darmstadt, 2010